Adıyaman University Journal of Science
https://dergipark.org.tr/en/pub/adyujsci
DergiPark AKADEMİK
ISSN 2147-1630
e-ISSN 2146-586X

Structural and Luminescence Characterization of $LiAlO_2$ Ceramics Synthesized by Sol-Gel Technique

Volkan ALTUNAL[1,*]

[1]*Cukurova University, Art Sciences Faculty, Department of Physics, 01250 Adana, TÜRKİYE*
valtunal@cu.edu.tr, ORCID: 0000-0001-9411-3441

Received: 24.05.2024 **Accepted:** 23.06.2024 **Published:** 28.06.2024

Abstract

This study aims to produce lithium aluminate ($LiAlO_2$) materials as dense ceramics by the sol-gel method and to examine their structural and luminescence properties for radiation dosimetry applications. The crystal structures of ceramics synthesized using the XRD method were confirmed and their morphological properties were examined using SEM analysis. The defect concentrations and lattice parameters of $LiAlO_2$ were also discussed in depth. It has been found that $LiAlO_2$ ceramics have a total of three exponential decay function components that decay OSL signals fast, medium and slow. The TL glow curve of the material exhibited two TL peaks located around 110 and 200 °C. An intense luminescence band around 700 nm was found in RL and TL emissions, which is attributed to oxygen vacancies in the structure. Obtaining promising luminescence signals for passive dosimetry from $LiAlO_2$ samples in this study may make them a candidate dosimeter for radiation dosimetry applications with further studies to be conducted in the future.

Keywords: $LiAlO_2$; Sol-Gel synthesis; Thermoluminescence; Optically stimulated luminescence; Radioluminescence.

* Corresponding Author DOI: 10.37094/adyujsci.1489596.

Sol-Jel Tekniği ile Sentezlenen $LiAlO_2$ Seramiklerinin Yapısal ve Lüminesans Karakterizasyonu

Öz

Bu çalışma, lityum alüminat ($LiAlO_2$) malzemelerinin sol-jel yöntemiyle yoğun seramikler halinde üretilmesini ve radyasyon dozimetri uygulamaları için yapısal ve lüminesans özelliklerinin incelenmesini amaçlamaktadır. XRD yöntemi kullanılarak, sentezlenen seramiklerin kristal yapıları doğrulandı ve malzemenin morfolojik özellikleri SEM analizi kullanılarak incelendi. $LiAlO_2$'nin kusur konsantrasyonları ve kafes parametreleri de derinlemesine tartışıldı. $LiAlO_2$ seramiklerinin OSL sinyalleri hızlı, orta ve yavaş bozulum sergileyen toplam üç üstel bozunma fonksiyonu bileşenlerine sahip olduğu bulunmuştur. Malzemenin TL ışıma eğrisi, 110 ve 200 °C civarında bulunan iki TL tepe noktası sergiledi. RL ve TL emisyonlarında yapıdaki oksijen boşluklarına atfedilen 700 nm civarında yoğun bir lüminesans bandı bulundu. Bu çalışmada $LiAlO_2$ örneklerinden pasif dozimetri için umut verici lüminesans sinyallerinin elde edilmesi, gelecekte yapılacak başka çalışmalarla onları radyasyon dozimetri uygulamaları için aday bir dozimetre haline getirebilir.

Anahtar Kelimeler: $LiAlO_2$; Sol-Jel sentezi; Termolüminesans; Optik uyarımlı lüminesans; Radyolüminesans.

1. Introduction

Thermoluminescence (TL) and Optical Stimulated Luminescence (OSL) are known as passive dosimetry methods and are based on luminescence emission following thermal or optical excitation of previously irradiated insulator or semiconductor materials, respectively [1]. Although the OSL method, which is a newer method compared to TL, offers great convenience in application, the number of OSL dosimetry systems is insufficient due to the newness of the technology [2, 3]. This situation has recently led researchers to develop new OSL dosimeters, and many alternative host materials have been proposed in the literature [4-9]. Carbon-doped alumina (Al_2O_3:C) is well known in personal dosimetry for its superior properties for medical physics applications [10]. It remains the material of choice despite its non-tissue equivalence to Al_2O_3:C (Zeff ~11.3), and non-sensitive to neutrons [11]. The way to develop a new OSL dosimeter could be a tissue-equivalent lattice. Moreover, certain critical properties are desirable in the development of materials with luminescent properties for OSL dosimetric applications. These include high radiation sensitivity, photosensitive trapped charges, linear behaviour in the dose-response relationship, minimal signal fading and resistance to external physical effects (e.g. mechanical stress and humidity). These properties are necessary to ensure that the material functions as an effective dosimeter.

Alkali aluminates are a lattice containing the elements alkali metals and aluminium, holding these two elements together with two oxygen atoms. The crystal structure of alkali aluminates can affect the placement of activator ions and the transitions between energy levels. Therefore, examining the luminescence properties of alkali aluminates is very important for optical and electronic applications [12-14]. Recently, their promising properties for LED applications, luminescence and imaging devices have been reported [15, 16]. In particular, $LiAlO_2$ is an important material for luminescence studies and dosimetric applications $LiAlO_2$ is also known to have high thermal stability and dosimetric properties that can be used to detect ionization radiation [12, 17, 18]. Therefore, the luminescence development and characterization of $LiAlO_2$ may offer an infrastructure for important applications for dose measurement and radiation detection in fields such as medical imaging, radiotherapy, and nuclear medicine [19, 20]. Additionally, $LiAlO_2$ with an effective atomic number of 10.7, making it the superior dosimetric material over Al_2O_3:C [21].

Although the luminescence sensitivity of pure $LiAlO_2$ has been reported to be low in the literature, the source of luminescence has not been fully identified, creating difficulties in optimizing and improving dosimetric properties. Therefore, in this study, $LiAlO_2$ ceramics were developed by the sol-gel method and their luminescence nature was examined in depth with RL, TL and OSL techniques.

2. Materials and Methods

2.1. Sample preparation

Figure 1 shows a simple schematic representation of the sol–gel pathway for $LiAlO_2$ ceramic pellets. The sol-gel route begins by dissolving nitrate-based Li and aluminium salts (purchased from Sigma Aldrich) in pure water in suitable molar ratios. After stirring for approximately 1 h at RT, citric acid (1:4, molar, purchased from Sigma Aldrich) was added to this mixture and the temperature was slowly increased to 80 °C. The dehydration process continued for approximately 24 hours. At the end of 24 hours, dried xerogel was achieved. 2-hour calcination treatment was applied at 900 °C to remove the organics that appeared in the structure during the formation of the crystal structure. As a result of the calcination route, pure $LiAlO_2$ white powders were obtained. $LiAlO_2$ powders were converted into 30 mg pellets using evacuable pellet dies in a manual pressing system before the sintering process. The dimensions of the prepared pellets were ~5.8 mm in diameter and ~0.70 mm in thickness. It should be noted that with the sintering treatment at 1300 °C for 4 hours, the mass of the ceramic pellets was measured to be approximately 24 - 24.8 mg. The final products were obtained as pellets with ~5.4 mm diameter and a ~0.5 mm thickness.

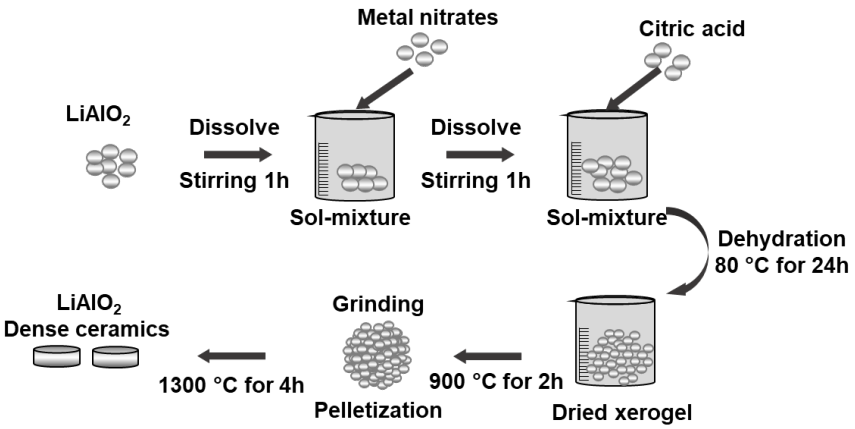

Figure 1: Schematic representation of the sol-gel process for $LiAlO_2$ ceramics

2.2. Characterization

To examine the structure and phase composition of $LiAlO_2$ crystals, X-ray diffraction (XRD) patterns were examined. The Panalytical Empyrean brand XRD analysis system used is equipped with a Cu-Kα tube, λ= 0.1541 nm. Patterns were investigated by scanning 0.02° with a 2θ scanning range from 10° to 90°. XRD ref. data from the International Center for Diffraction Data (ICDD) was used to identify crystalline phases.

The crystallite sizes of $LiAlO_2$ crystals were evaluated by the Debye-Scherrer formula [22];

$$D_{hkl} = K\lambda/(\beta_{hkl}cos\theta) \quad (1)$$

Here D refers to the crystallite size (nm); hkl are Miller indices; K is a numerical factor set at 0.9; λ represents wavelength; θ is half of the diffraction angle; and β is the full width at half maximum (FWHM), measured in radians.

Besides crystallite size, strain (ε) values were also calculated using the following equation [23]:

$$\varepsilon = \beta cos\theta/4 \quad (2)$$

where β is FWHM and θ represents half of the diffraction angle.

Another factor is the dislocation density (δ), which affects many properties of materials [24]. This density was determined by a special equation in $LiAlO_2$ crystals.:

$$\delta = 1/D^2 \quad (3)$$

where D represents the crystallite size of the $LiAlO_2$ crystals.

To examine the surface morphologies of $LiAlO_2$ ceramics, scanning electron microscope (SEM) photographs were taken using the Zeiss brand Supra 55 model SEM device. SEM photographs with

20000x direct magnification were obtained using 20 kV high voltage, and the grain size analysis of the surfaces was processed in the imageJ program.

2.3. Luminescence measurements

Luminescence signals of $LiAlO_2$ pellets were achieved using the DA-20 model Risø TL/OSL reader system of Danish origin. The system has a ^{90}Sr-^{90}Y radiation source (β) with 0.11 Gy/s. TL and OSL signals are captured with a EMI 9235QA PM tube. Hoya U-340 (100-400 nm permeability) filter was used in front of this PM tube. The OSL signals were acquired with 470 nm blue LED excitation. Prior to OSL readings, a preheating procedure was applied at 100 °C for 10 s to eliminate signals from unstable shallow traps. At the end of the OSL measurements, the samples were cleaned of residual doses by heating the samples to 450 °C with a heating rate of 5 °C/s. TL analyses were performed by heating the samples to 450 °C after irradiation with 2 °C/s, and background subtraction was necessarily applied. Background TL signals represent sample readings performed under the same conditions immediately after the initial TL reading.

Here, the analysis of OSL decay curves is based on a method based on fitting a combination of time decaying functions [25, 26]. The experimental OSL decay curve was analyzed by the first-order curve fitting. The fitting equation used for this analysis and representing the first-order kinetic approach can be written as following equation:

$$y = background + 1^{st}\ component + 2^{nd}\ component + 3^{rd}\ component + \cdots$$

$$I(t) = background + I_1 \exp\left(\frac{t}{\tau_1}\right) + I_2 \exp\left(\frac{t}{\tau_2}\right) + I_3 \exp\left(\frac{t}{\tau_3}\right) + \cdots \quad (4)$$

where 1^{st}, 2^{nd}, and 3^{rd} components refer to the first-order components of OSL signals that decrease with time, respectively. While t is the duration of stimulation; $I(t)$ is the OSL signal intensity as a function of time. $I_{1,2,3}$ and $\tau_{1,2,3}$ represent the maximum intensities and lifetimes, respectively. Deconvolution quality was evaluated by calculating Figure of Merit (FOM) values for the experimental curve [27].

Radioluminescence (RL) emission spectra were acquired in a homemade RL system consisting of a miniature X-ray source, a QE Pro-model Ocean Optics spectrometer, an X-ray control unit, and a closed chamber. While the samples were exposed to approximately ~20 kV X-rays, emissions in the range of 200 nm to 1000 nm were observed from the sample. TL emission measurements, performed in the range from 50 °C to 400 °C at a heating rate of 2 °C/s, were performed on a similar homemade TL spectrometer following a 600 s x-ray irradiation. This system consists of a monochromator, a sample holder with a linear heater, and a CCD camera mounted on the monochromator window (ANDOR). Despite the wide spectral coverage range of CCD cameras, TL emissions have been obtained in the

range of 400 nm to 1000 nm, as their quantum efficiency decreases significantly in the ultraviolet (UV) region, especially below 400 nm.

3. Results and Discussion

3.1. Structural and Morphological Properties

The phase formations of $LiAlO_2$ powders were confirmed through XRD analysis and are shown in Fig. 2. As seen from the figure, the XRD patterns matched well with the XRD peaks of the $LiAlO_2$ tetragonal (phase characterized by the P 41 21 2 space group) reference ICDD 98-003-0249 PDF card. The absence of any peak originating from any secondary phase confirms the $LiAlO_2$ phase, indicates that $LiAlO_2$ ceramics have been successfully synthesized.

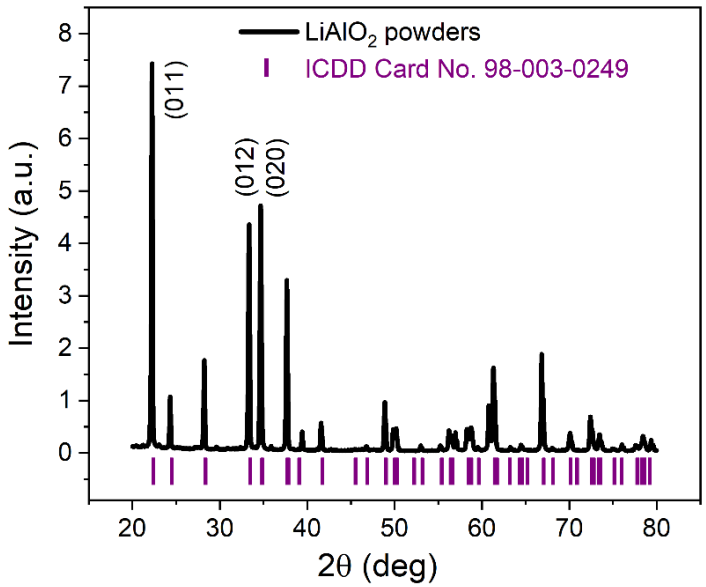

Figure 2: XRD pattern of the 1300 °C sintered $LiAlO_2$ powders prepared via sol-gel method

In Table 1, the Bragg angles represented with the three most intense diffraction peaks and the (011), (012), and (020), (hkl) planes are presented along with the structural parameters for the $LiAlO_2$ samples. The Eqn.1 was used to determine the crystallite size of each plane and the average crystallite size was calculated as 58.6 nm. In addition to the crystallite size, strain values were determined using the Eqn.2 for the (011), (012), and (020) planes and were found as 3.20×10^{-2}, 3.74×10^{-2}, and 3.74×10^{-2}, respectively. Another important parameter is the dislocation density (δ) values, which were found as 0.59×10^{20}, 0.41×10^{20}, and 0.41×10^{20} with the Eqn.3. As a result of phase analyses, it can be said that the crystallinity of $LiAlO_2$ powders are in compliance with the reference values and have good crystallinity.

Table 1. Positions of the diffraction peaks and structural parameters of $LiAlO_2$ powders

	hkl Planes		
	(011)	(012)	(020)
Peak Positions, 2θ, (°)	22.22	33.33	34.64
FWHM, β (°)	0.14	0.15	0.15
Crystalite size, D (nm)	64.92	55.51	55.42
Micro strain, ε x 10^{-2}	3.19	3.74	3.74
Dislocation density, δ (10^{20})	0.51	0.44	0.44

Figure 3 shows SEM photographs and particle size distribution histogram bars curves of $LiAlO_2$ powder and pellet samples. Here, after the calcination process of the powder samples, they were sintered at 1300 °C without pelletizing. As seen in Fig. 3, the pellet surfaces presented a more homogeneous structure than the morphology in the photographs obtained from powder samples. Relatively more irregularly, large and small structures were observed in the powder samples, and an increase in the distribution of the structures forming local necks was observed with the sintering treatment. On the other hand, as the particles of the pellet samples were fused together by pressure, relatively non-porous, smooth and interconnected smaller particle size clusters were observed on their surfaces with high temperature sintering.

The size distribution of the particles in the samples was determined by measuring them in the ImageJ program from SEM images that fit the well-known size histogram with the log-normal function. It should be noted that at least 200 particle sizes were measured during the evaluation. The obtained histograms and log-normal functions and the mean particle size (D) and standard deviation (σ_D) values of each sample are presented together with the SEM images of the corresponding samples in Fig. 3.

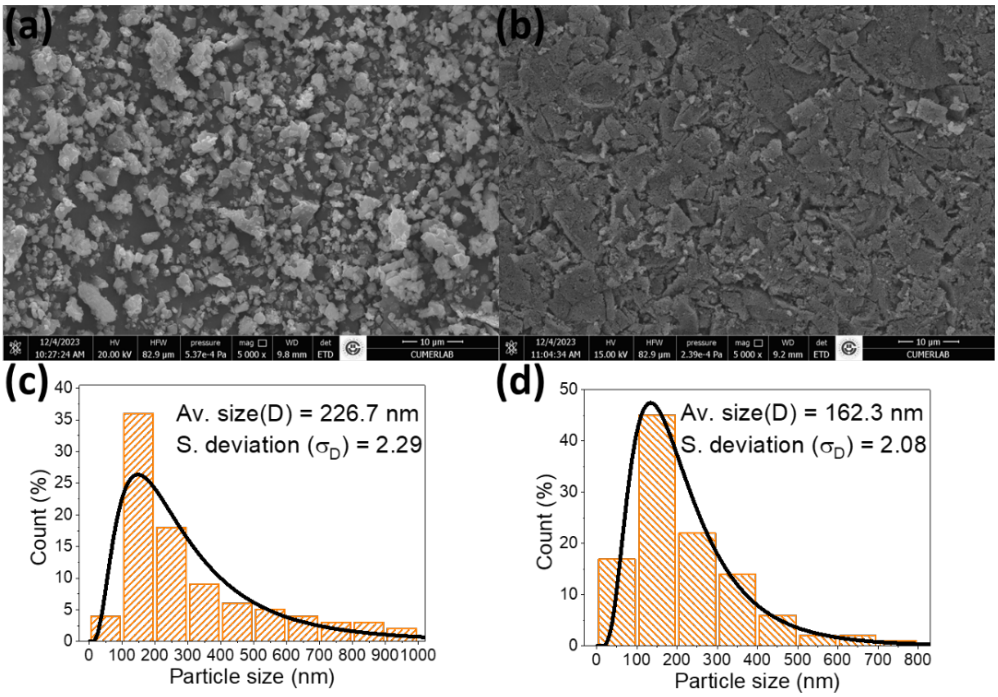

Figure 3: SEM micrographs of the $LiAlO_2$ samples in a) powder form, and b) pellet form; and the histogram (bars) with a log-normal function (red curve) to analyse the average size distribution for the $LiAlO_2$ samples in c) powder form, and d) pellet form

3.2. Luminescence Properties

Simple TL glow curves and OSL signals of $LiAlO_2$ pellets exposed to 1 Gy beta dose are shown in Fig. 4. The TL glow curves of $LiAlO_2$ pellets consist of a shoulder TL peak located at approximately 200 °C, followed by more delicate TL peak with a maximum located around 110 °C (see Fig. 4a). In the TL curves at higher temperatures, unstable signals caused by background subtraction are observed, so it is too early to talk about the existence of a significant TL trap in this region. On the other hand, the OSL decay curve of $LiAlO_2$ pellet exposed to 1 Gy is presented by log-log scales in Fig. 4b. After a preheating treatment at 100 °C/10 s, the obtained OSL signals exhibit two decaying parts (fast and slow), and the OSL signals come the background (zero) level in approximately 10 s. It can be said that $LiAlO_2$ pellets have sufficient sensitivity for personal and accident dosimetry studies that require relatively higher dose measurements.

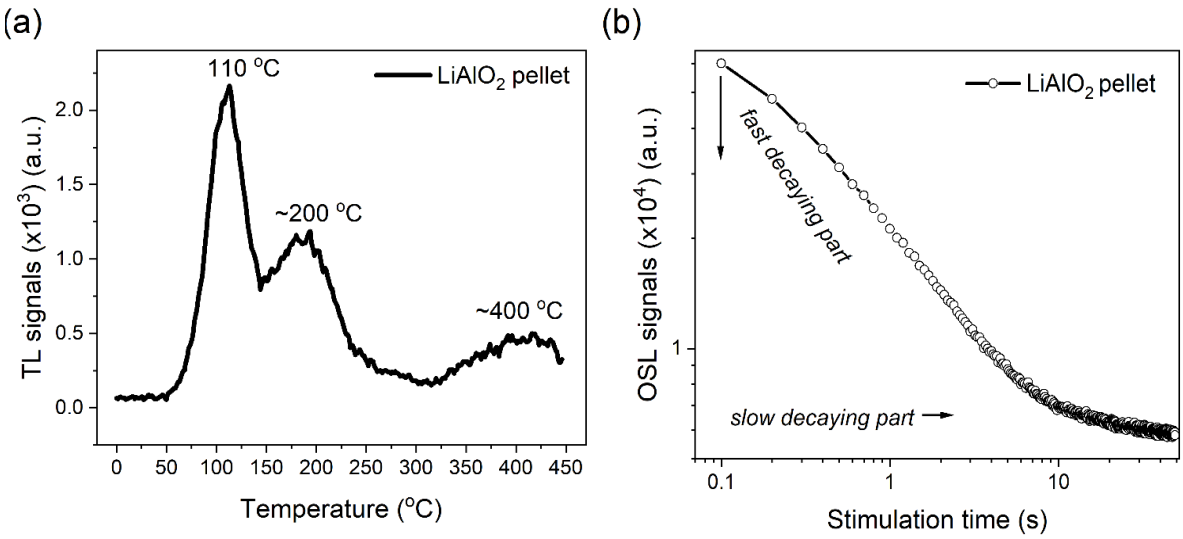

Figure 4: a) TL glow curve; b) OSL decay curve of the $LiAlO_2$ pellet sample. Sample was exposed to a beta dose of 1 Gy before TL and OSL readouts. Heating rate is 2 °C/s

Analysis of the OSL decay curve of $LiAlO_2$ is a crucial initial step to recognize the host material. Figure 5 shows the experimental OSL decay curve and their three first-order components analyzed via curve fitting. As can be seen from the figure, the OSL decay curve obtained from the $LiAlO_2$ pellet was well fitted to three time-decaying functions with an acceptable FOM value as 1.04. Undoubtedly, this OSL decay curve analysis method was also studied as the linear sum of two separate components, but when the fit quality was checked, the FOM value remained above 3.00. For this reason, three separate components were considered. It should be noted that this method is a simplified approach and does not provide precise information about actually existing trap levels and charge transfer.

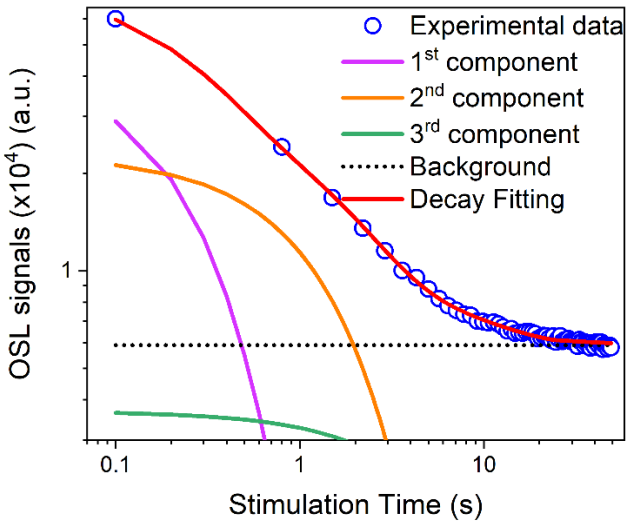

Figure 5: OSL decay curve and its components for the $LiAlO_2$ pellet samples which were previously irradiated with 1 Gy beta doses

RL emissions have been studied as a useful initial method providing information about the luminescence bands of dosimetric materials. Figure 6 shows the RL emission obtained from the sample during x-ray irradiation from 200 nm to 1000 nm. As can be seen from the figure, the emission of $LiAlO_2$ is represented by luminescence bands located in two different regions. It has a low sensitivity UV-Blue luminescence band located at 350 nm in the range from 200 to 500 nm and a broad luminescence band located at 740 nm between 600 nm and 850 nm towards the end of the visible region. There are many different speculations in the literature regarding the emission bands observed between 600 nm and 850 nm. While the emission band observed at 740 nm was attributed to the Fe^{3+} impurity unintentionally present in the Al_2O_3 used initially [28], it has also been suggested that some vacancy defects (such as large amounts of single-ion oxygen vacancies-surface disorder-oxygen interstitials-aluminium interstitials) at the deep levels of the band gap are responsible [4, 13, 29, 30].

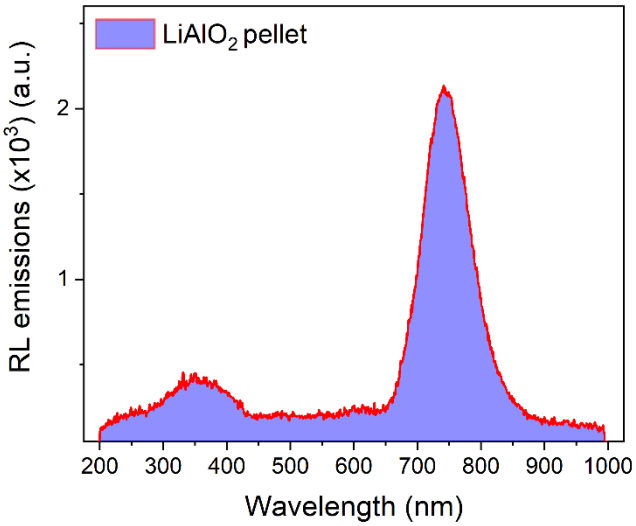

Figure 6: RL emissions of $LiAlO_2$ pellet

Figure 7 presents a contour plot of TL emission spectra obtained from $LiAlO_2$ pellet between 390 and 900 nm. As seen from the figure, a wide emission band around 740 nm dominates in TL emissions. It is seen that TL traps are close to each other and overlap between 100 °C and 300 °C. Comparing the RL and TL emissions in the range of 400 nm to 900 nm, it is found that the TL and RL emissions are almost the same. This may mean that similar recombination centres are involved in luminescence in both luminescence processes. The actual luminescence mechanism is undoubtedly much more complex. Here, with simplified approximations, it can be inferred that after the radiation dose, charge-trapped carriers in the intrinsic defects of $LiAlO_2$ (oxygen vacancies, surface defects, etc.) result in the emissions observed by electron/hole recombination in V-type defects.

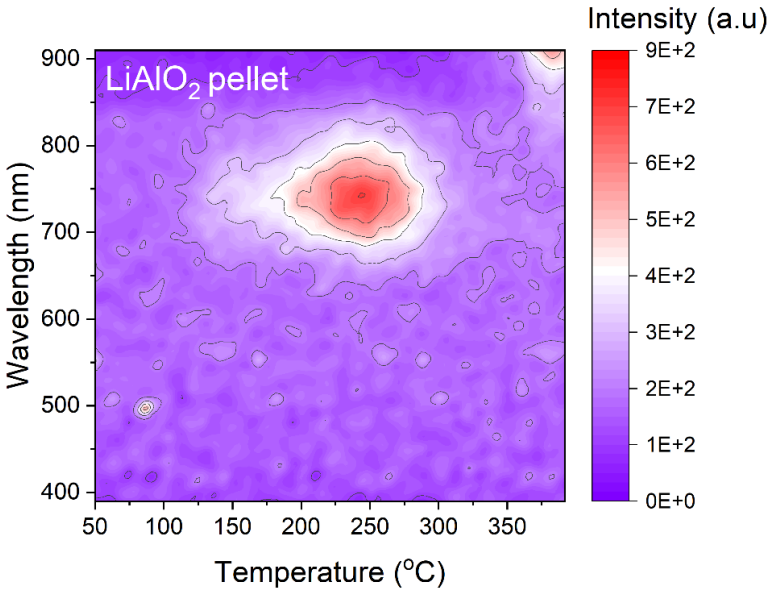

Figure 7: The colour map plot of the TL emission (390–900 nm) of $LiAlO_2$ pellet after 600 s excitation.

4. Conclusion

This study revealed the production, structural and morphological characterization, and luminescence properties of $LiAlO_2$ material, a promising host material for OSL dosimetry, using the sol-gel synthesis method. $LiAlO_2$ crystals were successfully synthesized by the sol-gel method in the tetragonal phase, and in SEM analysis, it was observed that the grain sizes of the powder samples decreased with the pelletization process and ceramic structures with smooth surface forms were obtained. $LiAlO_2$ pellets offered promising OSL response in the UV region, although their TL sensitivity was low. It was concluded that the RL and TL emission luminescence bands obtained between 400 and 900 nm were similar and they may be using the same recombination centers. $LiAlO_2$ is a suitable host to produce more sensitive luminescent materials in OSL dosimetry. With this study, the luminescence source of $LiAlO_2$-based materials was identified and it was concluded that they can be used in dose measurement in radiation measurement applications with future doping studies.

Acknowledgements

This study was supported financially by the Çukurova University Research Projects Development and Coordination Unit under contract number FKB-2023-16411. Therefore, I am grateful to the Rectorate of Çukurova University for their financial support. I thank Prof. Kasım Kurt and Özlem Yiğit from Mersin University for their valuable contributions to RL and TL emission measurements.

References

[1] Bøtter-Jensen, L., McKeever, S.W.S., Wintle, A.G., *Optically stimulated luminescence dosimetry*, *1st ed*, 355 pp, Elsevier, 2003.

[2] McKeever, S.W.S., Moscovitch, M., *On the advantages and disadvantages of optically stimulated luminescence dosimetry and thermoluminescence dosimetry*, Radiation Protection Dosimetry, 104(3), 263-270, 2003.

[3] Akselrod, M.S., Bøtter-Jensen, L., McKeever, S.W.S., *Optically stimulated luminescence and its use in medical dosimetry*, Radiation Measurements, 41(1), 78-99, 2006.

[4] Altunal, V., Guckan, V., Ozdemir, A., Yegingil Z., *A calcination study on BeO ceramics for radiation dosimetry*, Materials Research Bulletin, 130, 110921, 2020.

[5] Ozdemir, A., Altunal, V., Guckan, V., Kurt, K., Yegingil Z., *Luminescence characteristics of newly-developed $MgB_4O_7:Ce^{3+},Na^+$ phosphor as an OSL dosimeter*, Journal of Alloys and Compounds, 865, 158498, 2021.

[6] Altunal, V., Ozdemir, A., Kurt, K., Yigit, O., Guckan, V., Isik, B., Yegingil Z., *Luminescence properties of Ce and Be-doped $CaAl_{12}O_{19}$ for dosimetric and light-emitting applications*, Journal of Alloys and Compounds, 985, 174081, 2024.

[7] Guckan, V., Altunal, V., Ozdemir, A., Yegingil Z., *Optically stimulated luminescence of MgO:Na,Li phosphor prepared using solution combustion method*, Journal of Alloys and Compounds, 835, 155253, 2020.

[8] Ozdemir, A., Guckan, V., Altunal, V., Kurt, K., Yegingil Z., *Thermoluminescence in MgB_4O_7:Pr,Dy dosimetry powder synthesized by solution combustion synthesis method*, Journal of Luminescence, 230, 117761, 2021.

[9] Nur, N., Guckan, V., Kizilkaya, N., Depci, T., Ahmedova, C., Ozdemir, A., Altunal, V., Yegingil Z., *Thermoluminescence properties of non-stoichiometric $Li_2Si_2O_5$ synthesized from natural amethyst quartz*, Journal of Luminescence, 179, 366-371, 2016.

[10] McKeever, S.W.S., Akselrod, M.S., Colyott, L.E., Agersnap Larsen, N., Polf, J.C., Whitley, V., *Characterisation of Al_2O_3 for use in thermally and optically stimulated luminescence dosimetry*, Radiation Protection Dosimetry, 84(1-4), 163-166, 1999.

[11] Akselrod, M.S., Lucas, A.C., Polf, J.C., McKeever, S.W.S., *Optically stimulated luminescence of Al_2O_3*, Radiation Measurements, 29(3-4), 391-399, 1998.

[12] Dhabekar, B., Raja, E.A., Menon, S., Gundu Rao, T.K., Kher, R.K., Bhatt,nB.C., *Identification of defect centres using TSL, PL, OSL and ESR studies in $LiAlO_2$ based phosphors*, Journal of Physics D: Applied Physics., 41, 115414, 2008.

[13] Jopat, P.R., Sisodiya, D.S., Sen, S., M.S. Kulkarni, *$LiAlO_2$:Sm a highly sensitive and multi-functional radiation dosimeter*, Ceramics International, 48(24), 36593-36600, 2022.

[14] Wani, M.A., Dhoble, S.J., Belekar, R.M., *Synthesis, characterization and spectroscopic properties of some rare earth activated $LiAlO_2$ phosphor*, Optik, 226(1), 165938, 2021.

[15] Bajaj, N.S., Omanwar, S.K., *LEDs phosphor $BaAl_2O_4$:Sm prepared by solution combustion synthesis*, AIP Conference Proceedings, 1536(1), 803-804, 2013.

[16] Poort, S., Blokpoel, W.P., Blasse, G., *Luminescence of Eu^{2+} in barium and strontium aluminate and gallate*, Chemistry of Materials, 7(8), 1547-1551, 1995.

[17] Agarwal, M., Garg, S.K., Asokan, K., Kumar, P., *Temperature-dependent OSL properties of nano-phosphors $LiAlO_2$:C and α-Al_2O_3:C*, Applied Surface Science, 444, 819-828, 2018.

[18] Lee, J.I., Pradhan, A.S., Kim, J.L., Chang, I., Kim, B.H., Chung, K.S., *Characteristics of $LiAlO_2$–Radioluminescence and optically stimulated luminescence*, Radiation Measurement., 56, 217-222, 2013.

[19] Dickens, P.T., Marcial, J., McCloy, J., McDonald, B.S., Lynn, K.G., *Spectroscopic and neutron detection properties of rare earth and titanium doped $LiAlO_2$ single crystals*, Journal of Luminescence, 190, 242-248, 2017.

[20] Takebuchi, Y., Watanabe, K., Nakauchi, D., Fukushima, H., Kato, T., Kawaguchi, N., Yanagida, T., *Scintillation properties of Ce-doped $LiAlO_2$ for neutron detection*, Journal of the Ceramic Society of Japan, 129(7), 397-401, 2021.

[21] Twardak, A., Bilski, P., Marczewska, B., Lee, J.I., Kim, J.L., Gieszczyk, W., Mrozik, Sądel, A., M., Wróbel, D., *Properties of lithium aluminate for application as an OSL dosimeter*, Radiation Physics and Chemistry, 104, 76-79, 2014.

[22] Klug, H.P., Alexander, L.E., *X-ray diffraction procedures: for polycrystalline and amorphous materials, X-Ray Diffraction Procedures: For Polycrystalline and Amorphous Materials*, *2nd ed*, 992 pp, Wiley, 1974.

[23] Norazlina, M.S., Shanmugan, S., Mutharasu, D., *Structural Analysis of BeO Nanoparticles Synthesized by Polyacrylamide Gel Route*, Advanced Science Focus, 1, 362-366, 2013.

[24] Theivasanthi, T., Alagar, M., *Electrolytic synthesis and characterizations of silver nanopowder*, Nano Biomedicine and Engineering, 4(2), 58-65, 2012.

[25] Altunal, V., Yegingil, Z., Tuken, T., Depci, T., Ozdemir, A., Guckan, V., Nur, N., Kurt, K., Bulur, E., *Optically stimulated luminescence characteristics of BeO nanoparticles synthesized by sol-gel method*, Radiation Measurements, 118, 54-66, 2018.

[26] Altunal, V., Guckan, V., Ozdemir, A., Zydhachevskyy, Y., Lawrence, Y., Yu, Y., Yegingil, Z., *Three newly developed BeO-based OSL dosimeters*, Journal of Luminescence, 241, 118528, 2022.

[27] Balian, H.G., Eddy, N.W., *Figure-of-merit (FOM), an improved criterion over the normalized chi-squared test for assessing goodness-of-fit of gamma-ray spectral peaks*, Nuclear Instruments and Methods, 145, 389-395, 1977.

[28] Pejchal, J., Fujimoto, Y., Chani, V., Yanagida, T., Yokota, Y., Yoshikawa, A., Nikl, M., Beitlerova, A., *Modifications of micro-pulling-down method for the growth of selected Li-containing crystals for neutron scintillator and VUV scintillation crystals*, Journal of Crystal Growth, 360, 127-130, 2012.

[29] Li, P.G., Lei, M., Tang, W.H., *Raman and photoluminescence properties of α-Al_2O_3 microcones with hierarchical and repetitive superstructure*, Materials Letters, 64(2), 161-163,2010.

[30] Tavernier, S., Gektin, A., Grinyov, B., Moses, W.W., *Radiation detectors for medical applications*, *1st ed,* 307 pp, Springer Dordrecht, 2006.